geosciences

MDPI

Article

The Mechanical Characterization of Pyroclastic Deposits for Landslide Early Warning Systems

Emilia Damiano [1,*], Martina de Cristofaro [1], Antonia Brunzo [1], Goffredo Carrieri [2], Luisa Iavazzo [1], Nadia Netti [3] and Lucio Olivares [1]

[1] Department of Engineering, University of Campania "Luigi Vanvitelli", 81031 Aversa, Italy; martina.decristofaro@unicampania.it (M.d.C.); antonia.brunzo@unicampania.it (A.B.); ing.iavazzo@gmail.com (L.I.); lucio.olivares@unicampania.it (L.O.)
[2] Italian Air Force, Viale dell'Università, 00118 Rome, Italy; goffredo.carrieri@aeronautica.difesa.it
[3] Department of Economics, Management and Institutions, University of Napoli "Federico II", 80138 Naples, Italy; nadia.netti@unina.it
* Correspondence: emilia.damiano@unicampania.it; Tel.: +39-081-5010262

Abstract: Broad mountainous areas in the western Campania (southern Italy), where young pyroclastic deposits extensively outcrop, frequently experience rainfall-induced slope movements of different degrees of mobility, causing heavy damage and fatalities. Such landslides cannot be easily mitigated, and the implementation of physically based early warning systems is still not able to predict the post-failure evolution of slope movements and the exposed areas at risk. This paper is devoted to overcoming this limit. To this end, the mechanical characterization of pyroclastic soil, carried out through an extensive laboratory testing program, is presented and compared with those of two other ashy soils of different depositional mechanisms. The results show that the depositional mode influences soil properties; to begin with, it affects the unsaturated shear strength, whose intercept of cohesion is up to 5 kPa higher in ashes of flow deposition than in airfall ash deposits. The saturated undrained soil response allowed for the identification of different levels of susceptibility to the liquefaction of pyroclastic deposits, which is one of the main factors governing the post-failure evolution of landslides. Gathering all the acquired information, including saturated and unsaturated soil shear strength, permeability function, and water retention curves, into a soil database, it was possible to present all data under a unitary framework. Finally, the implementation of the proposed flowchart for a simplified assessment of post-failure evolution to be employed in regional early warning systems can enhance our knowledge of the areas at risk.

Keywords: rainfall-induced landslide; pyroclastic soils; unsaturated soil mechanics; liquefaction; early warning systems

Citation: Damiano, E.; de Cristofaro, M.; Brunzo, A.; Carrieri, G.; Iavazzo, L.; Netti, N.; Olivares, L. The Mechanical Characterization of Pyroclastic Deposits for Landslide Early Warning Systems. *Geosciences* **2023**, *13*, 291. https://doi.org/10.3390/geosciences13100291

Academic Editors: Jesus Martinez-Frias and Hans-Balder Havenith

Received: 10 August 2023
Revised: 11 September 2023
Accepted: 20 September 2023
Published: 23 September 2023

1. Introduction

A significant part of the Campanian slopes (southern Italy) is covered by young deposits arising from the recent explosive activity of the Somma–Vesuvius and Phlaegrean Fields volcanic centers present in the area. They have generated pyroclastic deposits of different thicknesses and characteristics depending on the distance from the eruptive centers and on deposition mechanisms (airfall, flow, or surge deposits), which mantled steep slopes present in a wide area around the Campanian Plain. Over the years, these covers were subjected to numerous shallow landslides due to infiltration processes following prolonged and intense rainfalls. The stability of these shallow slopes is mainly due to the unsaturated conditions of the covers: the presence of matric suction causes an apparent cohesive intercept, which increases the soil shear resistance [1]. During rainwater infiltration, the increase in soil weight and the decrease in matric suction may lead to slope instabilities [2–4]. Some of them evolved into catastrophic flowslides able to run for kilometers even over flat areas, destroying entire population centers and causing numerous fatalities [2,5].

Such landslides cannot be easily mitigated owing to their complexity and their large areal extension; therefore, one of the strategies used to face them is the implementation of physically based early warning systems capable of simulating the triggering phenomena [6–8]. However, these systems are available for analysis at the slope scale, and usually, they are not able to predict the evolution of subsequent movements. To overcome this limitation, a first attempt was made in [9], where the authors suggested developing a soil database (SDB) for implementation in regional landslide early warning systems, based on advanced constitutive models. In addition to the main morphological characteristics of the slopes, the information in the database includes data on the mechanical properties of the soils in both saturated and partially saturated conditions as well as the assessment of their susceptibility to liquefaction, which is considered to play a role in the evolution of landslides into flowslides [10,11]. The database only includes airfall deposits lying on limestone bedrock involved in previous catastrophic flowslides. In many cases, however, the rapid landslides that affect some shallow covers around Naples do not evolve into flowslides. In this case, the sliding mass shows less mobility and, usually, stops along the slope or at its toe. This kind of phenomenon can involve pyroclastic deposits formed through different deposition mechanisms, like pyroclastic flows, lying on a bedrock of different nature. The aim of this work is to extend the knowledge framework by analyzing also the pyroclastic deposits involved in slope movements that do not eevolve into flowslides.

In particular, this paper shows the results of an extensive laboratory experimental program performed in both saturated and unsaturated conditions on a flow deposit present along a hill near the city of Naples and recurrently involved in rainfall-induced landslides with no flow-like characteristics. The obtained results contribute to the enrichment of the database first proposed by [9]. Moreover, by comparing the characteristics of the deposit herein analyzed with those of deposits involved in flowslides (Sarno and Cervinara), it is possible to highlight the similarities and dissimilarities between the two types of soil deposits and enhance the comprehension of the mechanisms that govern the post-failure evolution of shallow rainfall-induced slope movements. Finally, this study aims to gather all the acquired information in a flowchart for a simplified assessment of the post-failure evolution of landslides.

The SDB and the proposed flowchart provide the features necessary to improve the existing EWSs whose reliability depends on adopting realistic hydro-geotechnical models (e.g., for unsaturated soils) that enable researchers to detect triggering thresholds, thus minimizing the risk of false or late alarms. Although the extension of such a database to the regional scale requires a major effort, which may be considered costly for the community, undoubtedly, many economic benefits are derived from the use of well-calibrated physically based models in the implementation of EWSs.

2. Background

From a geomorphological point of view, the Campania region is very complex and can be divided into macro-areas depending on the nature of the bedrocks (volcanic, carbonate, terrigenous, and alluvial) [12] (Figure 1a).

The deposits covering these areas consist of pyroclastic materials, accumulated after the eruptions of the volcanic centers of Roccamonfina, Phlaegrean Fields, and Somma-Vesuvius. They can be categorized into air-fall, flow, or surge deposits, and although originating from the same volcanic eruptions, they take on different physical and mechanical characteristics depending on the distance from the eruptive centers and transport, accumulation, and deposition processes. Airfall deposits are formed by pyroclastic particles directly ejected from the crater in the form of a sustained eruptive column that, after wind transport,, fall down mantling slopes and plains. Due to transport and deposition modes, the particles have sharp edges, as they are not abraded by dragging mechanisms. By contrast, surge and flow deposits are generated as a result of the sedimentation of eruptive mixtures composed of solid particles and gases that flow along the sides of the volcano.

These particles have rounded edges due to being subjected to abrasion they undergo during sliding. Surge deposits have less heterogeneous and smaller granule sizes than those constituting flow deposits. Surge deposits often contain small, rounded structures, called pisolites, comprising ash particles. The substantial difference between flow and surge deposits is the different percentage of the aeriform component, which is greater in surge deposits [13].

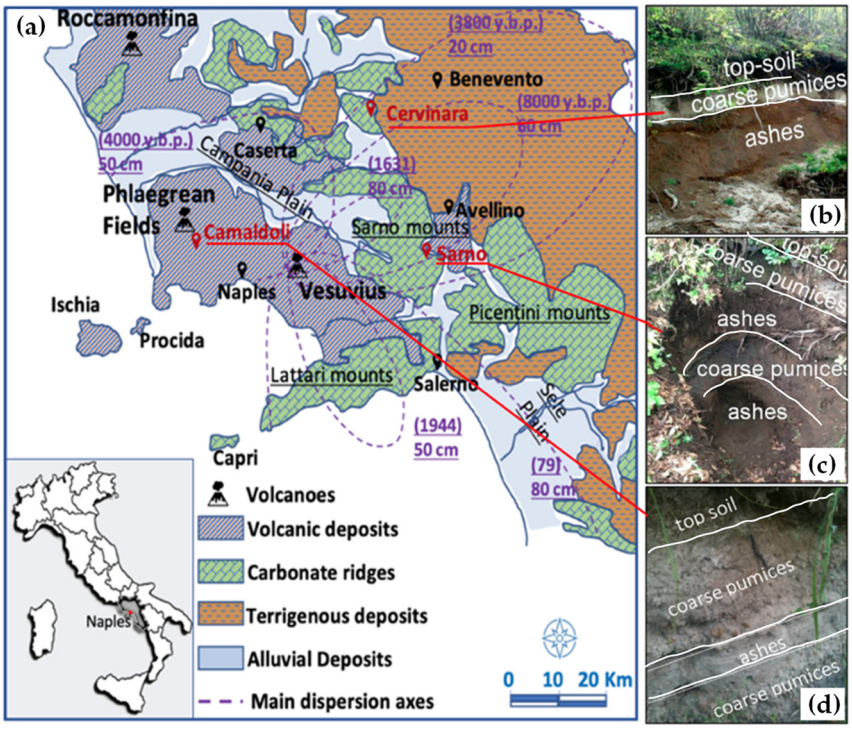

Figure 1. (**a**) Geomorphological contexts of the pyroclastic deposits in Campania, Italy; schematic stratigraphy at the location of the study sites: (**b**) Cervinara; (**c**) Sarno; (**d**) Camaldoli.

In recent years, the scientific community has shown considerable interest in the landslide events of Campania along the slope covered by airfall pyroclastic deposits that evolved into flowslides. Notably, significant attention has been given to the Sarno and Cervinara sites (Figure 2), where catastrophic flowslides occurred in 1998 and 1999, respectively. In this geomorphological context, defined henceforth as "carbonatic context", slope failures involve airfall pyroclastic deposits in a primary position lying on fractured limestone bedrock [14]. Covers consist of alternating layers of loose ash and pumice: they are regularly layered, with thicknesses ranging between 0.5 and 3 m in the detachment zone and inclination between 30 and 40°.

In this paper, instead, our focus will also be on the slopes surrounding the city of Naples in the Phlegrean area, where landslides are characterized by the accumulation of the landslide body at the toe of the slopes (Figure 2). Along these slopes, numerous landslides occur about every year, which, although characterized by a degree of mobility lower than flowslides, cause engineering problems to surrounding structures and infrastructure, as they are very close to highly urbanized areas. The covers involved are generally in primary position; however, differently from those involved in flowslides, they consist of flow or surge pyroclastic deposits. In this "volcanic context", the nature of bedrock is different; it is mainly constituted by lava, tuff, and weakly cemented pyroclastic materials, as well as slope inclinations in the detachment areas, which reach a value as high as 60° (Camaldoli and Agnano hills) (Figure 2). Moreover, the covers show a less regular stratigraphic sequence: alternations of paleosoils and loose soils (ash, pumice, and scoriae) (Figure 1d) reach tens of meters on the top of the slope. In this case, shallow landslides develop in the most superficial portion of the soil cover, with a thickness ranging from tens of cm to almost

1–2 m [15]. According to [14,16], landslides triggered in the volcanic context usually evolve into small slides or debris avalanches and propagate, with a travel distance usually no more than 300 m, while in the carbonatic context, large flowslides or debris avalanches develop, which generally propagate over distances as long as several kilometers.

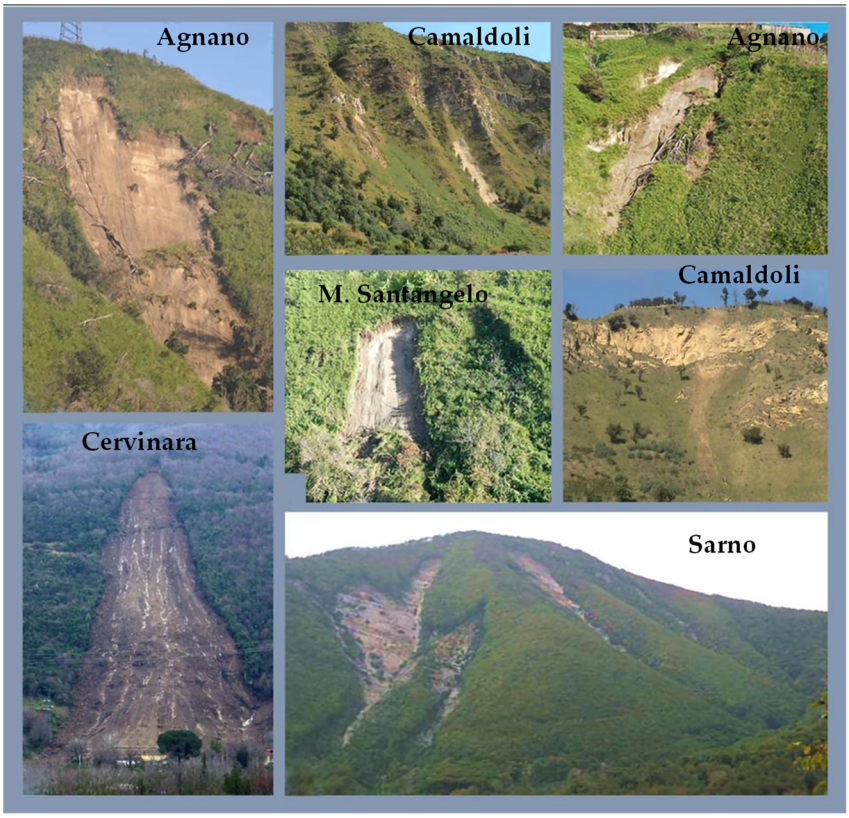

Figure 2. Landslides case history in pyroclastic covers (Campania region).

Hence, the assessment of the post-failure evolution remains a key point for hazard mapping in these areas. In this regard, and considering the simplified hypothesis of homogeneous infinite slope in cohesionless soil, Ref. [3] implemented a flowchart for a simplified assessment of landslide evolution, pointing out that the post-failure evolution of a landslide is strictly related to the degree of saturation at the onset of instability and the susceptibility of the involved soil to liquefaction. Along steep slopes, characterized by an inclination almost equal to the friction angle of the soil ($\alpha \cong \phi'$), after intense precipitation, failure occurs in conditions close to saturation ($Sr \cong 1$). Under these conditions, in soil deposits susceptible to liquefaction, the evolution of the landslide into a flowslide is associated with the undrained instability (static liquefaction) that occurs in saturated loose granular soils under shear stress. In soil deposits not susceptible to liquefaction, the mechanisms underlying the post-failure evolution associated with the development of undrained response are essentially debris avalanches or slides. On very steep slopes ($\alpha >> \phi'$), failure occurs when the soil is far from a saturated condition ($Sr << 1$). In this case, the slope movement evolves into a debris avalanche or slide, independently from the eventual susceptibility to the liquefaction of the involved soils because the partially saturated condition prevents the development of an undrained response. Nevertheless, a comprehensive investigation of the mechanical properties of the soil cover is needed to effectively evaluate the triggering and post-failure mechanisms of rainfall-induced landslides in pyroclastic deposits.

To this aim, an extensive experimental program on pyroclastic soil, taken from a flow deposit located in the surrounding of Naples, was carried out to frame the saturated soil response within the steady-state theory and define soil susceptibility to the liquefaction of the deposit. Partial saturation conditions were also analyzed to assess the influence of

the degree of saturation on soil shear strength and evaluate the water retention curve and permeability function. The experimental results shed light on the possibility of enriching the database for early warning system implementation [17,18] by adding the data of soil belonging to a pyroclastic deposit of flow or surge origin lying on volcanic bedrock to the database.

3. Materials and Methods

The Camaldoli slope was chosen as representative of a flow deposit generated near the eruptive center of Phlegrean Fields. The hill, located to the north of the city, is the highest relief of Naples. The south-facing side is characterized by steep slopes of tuff rocks, while the north-facing side presents gentler slopes covered by a wooded area. As reported by [15], the hill can be ideally subdivided into four different parts: the top high plain, characterized by local acclivity higher than 60°, bounded at its lower limit by the vertical cliff of tuff rock; the main slope with an inclination between 30° and 50°; the foot slope and the basal plain where the steepness becomes lower. Detachment areas are usually present at the highest altitudes of the slope above the vertical tuff cliff, where the thickness of the cover is very small.

The study area is in the upper part of the south-facing slope near the "Camaldoli hermitage" in an area characterized by slope angles ranging between 40 and 60°. Here, the slope is covered by a soil deposit tens of meters thick lying on volcanic bedrock consisting of yellow Neapolitan tuff.

The undisturbed samples used in the experimental program were taken in a 1.5 m deep recess cut along a subvertical escarpment excavated for the construction of a road that crosses the slope at a depth of about 4–6 m from the top. In this way, it was possible to identify and collect soils in primary deposition. To minimize disturbances, the soil specimens were directly taken with thin-wall metal samplers (Figure 3) having the same size as laboratory equipment used for studying the specimens (38 mm and 68 mm).

Figure 3. Example of manual undisturbed sampling.

The mean values of the physical properties of the sampled soils are reported in Table 1 in terms of the maximum diameter of soil d_{max}, the specific unit weight of the soil particles γ_s, the unit weight of soil volume γ, porosity n, and the degree of saturation S_r. The soil is characterized by a low specific unit weight of about 25 kN/m^3, probably due to the presence of internal voids of the soil particles, by porosity ranging between 53% and 55% and a saturation degree ranging between 24% and 46% related to the weather conditions.

Table 1. Main physical properties of Camaldoli ash.

d_{max} (mm)	γ_s (kN/m^3)	γ (kN/m^3)	n (%)	S_r (%)
6	24.9	12.0	53–55	24–46

The grain size distribution of the soil, illustrated in Figure 4, shows that it can be classified as silty sand. The uniformity coefficient is about 10, showing a quite uniform particle size distribution. Visual observation allows for the recognition of particles with rounded edges because of the abrasion that occurs during the formation of flow deposits.

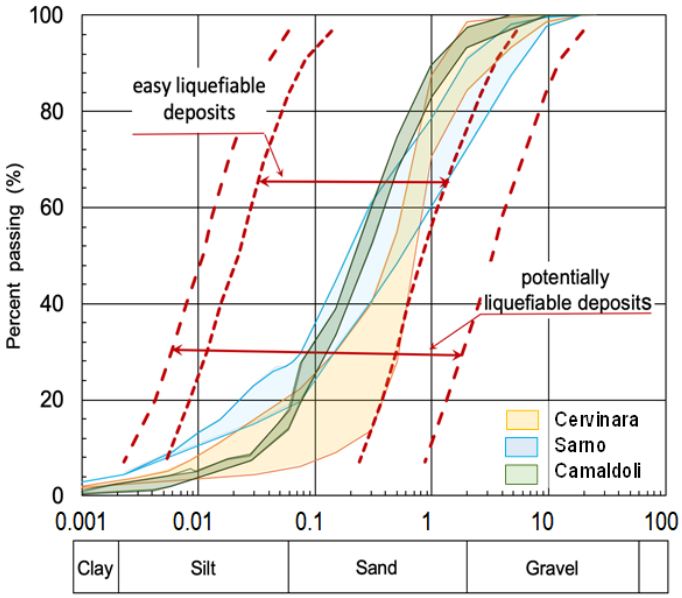

Figure 4. Grain size distribution of Camaldoli ash compared with other liquefiable ash deposits of Campania and with the bounds of liquefiable natural soil deposits.

In the same Figure 4, the grain size distribution of the Camaldoli ash is compared with the bounds of natural deposits susceptible to liquefaction under monotonic and cyclic loading [19] as well as with the bounds of Cervinara and Sarno deposits. It should be noted that the Camaldoli ash is included in the range of easily liquefiable deposits. Therefore, from this preliminary analysis, the soil can be defined as potentially liquefiable.

To define the mechanical properties of the soil in both saturated and unsaturated conditions, a comprehensive laboratory testing program was carried out, which consisted of the following tests:

- Consolidated isotropically drained and undrained (CID and CIU) triaxial tests on saturated specimens to evaluate soil shear strength and susceptibility to liquefaction;
- Constant head permeability test to determine the saturated hydraulic conductivity;
- Suction-controlled triaxial tests (SCTX) on undisturbed specimens to define hydraulic conductivity function and evaluate the effects of partial saturation on shear strength;
- Infiltration/evaporation method for the evaluation of the soil water retention curve (SWRC).

4. Results

4.1. Mechanical Properties in Saturated Conditions

4.1.1. Saturated Shear Strength and Undrained Response

The mechanical response of the Camaldoli ash was investigated through CID and CIU tests performed on undisturbed natural soil samples saturated by adopting the experimental technique proposed by [20]. After soil saturation, specimens were isotropically consolidated under mean effective stresses between 25 kPa and 300 kPa. The void ratios at the end of the consolidation phases ranged between 1.1 and 1.2 (Table 2) [21].

Table 2. Triaxial tests in saturated conditions: state parameters at the end of the consolidation stage and the applied mean effective stress [21].

Test ID	γ (kN/m^3)	γ_d (kN/m^3)	w (%)	n (%)	e	p'_0 (kPa)
C_Cid_1	16.9	11.5	46.5	53.6	1.16	73.4
C_Cid_2	17.0	11.7	45.4	53.1	1.13	99.38
C_Cid_3	17.0	11.8	44.4	52.7	1.11	147.66
C_Cid_4	16.7	11.6	42.9	53.3	1.14	149.86
C_Cid_5	16.7	11.4	47.2	54.4	1.19	25.85
C_Cid_6	16.9	11.7	45	53.1	1.13	229.5
C_Cid_7	16.6	11.2	48	54.9	1.22	49.56
C_Cid_8	16.9	11.5	46.8	53.7	1.16	125.67
C_Ciu_1	17.1	11.9	43.1	52.1	1.09	297.46
C_Ciu_2	16.8	11.6	44.2	53.2	1.14	34.69
C_Ciu_3	17.0	11.7	44.7	52.8	1.12	69.97
C_Ciu_4	17.1	11.9	44	52.3	1.10	220.11
C_Ciu_5	16.9	11.8	43.5	52.7	1.12	126.69
C_Ciu_6	17.0	11.8	44.2	52.7	1.12	99.83
C_Ciu_7	17.0	11.9	42.8	52.3	1.10	148.01
C_Ciu_8	17.0	11.9	42.6	52	1.09	199.99

The results of both types of tests are reported in Figure 5 in terms of stress paths (the p′–q plane in Figure 5a), the evolution of deviatoric stress (the ε_a–q plane in Figure 5b,c), the evolution of volumetric strain during CID test (the ε_a–ε_v plane in Figure 5d), and the development of excess pore pressure during undrained CIU test (the ε_a–Δu plane in Figure 5e).

In drained conditions, the soil shows a fragile behavior (Figure 5a,b): the mobilized strength first reaches a peak value and then stabilizes at a lower critical state value. The corresponding strength parameters are as follows:

- A friction angle equal to 38° and cohesion of 15 kPa at peak;
- A friction angle of 38° and cohesion of 0 kPa at the critical state.

The soil has a high friction angle and a relatively low effective cohesion in the investigated stress field.

In undrained conditions (green lines in Figure 5a,c), the stress paths clearly show that, with an increase in deviatoric stress, partial instability occurs, with an initial decrease in the mean effective stress and a subsequent progressive increase (transformation phase point) until a larger final value of deviatoric stress is reached under a high level of strain. The soil, therefore, shows a potentially non-liquefiable behavior.

The results are reported in the compression plane (log p′–e) in Figure 6. In detail, the points represent the final state of the specimens in CID tests and both the initial and final conditions of the specimens in CIU tests. The final conditions fall under a narrow range of values (highlighted in red in Figure 6), which allows for the identification of the steady-state conditions and the position of the steady-state line (SSL) in the compression plane. The SSL is almost straight and is characterized by a slope slightly higher than the isotropic compression line, shown in the same figure (green line).

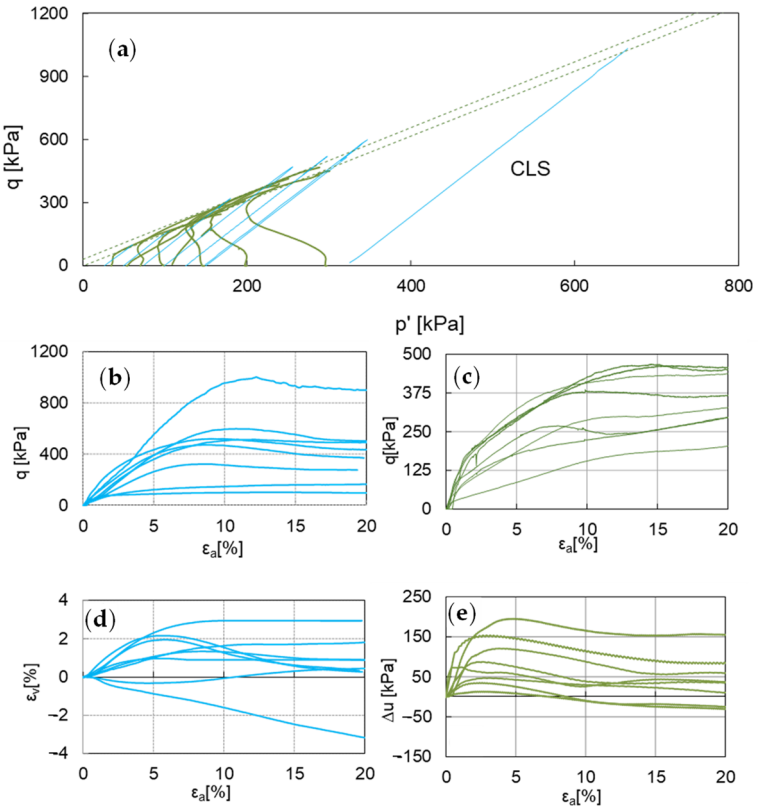

Figure 5. Triaxial test results: (**a**) stress plane; (**b**) results of CID tests in εa–q plane; (**c**) results of CIU tests in εa–q plane; (**d**) results of CID tests in εa–εv plane; (**e**) results of CIU tests in εa–Δu plane.

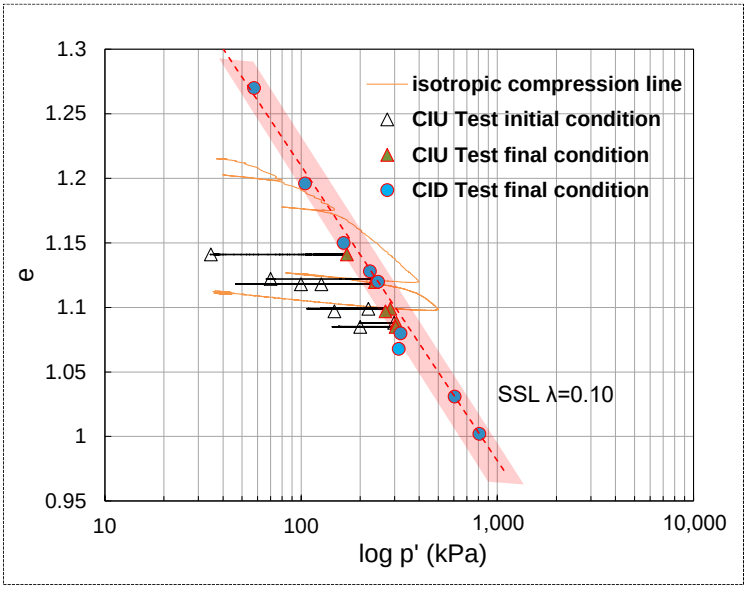

Figure 6. Triaxial test results: compression plane.

In framing the undrained soil behavior through the lens of the steady-state theory [22], we can use the SSL as a discriminating factor to verify soil susceptibility to liquefaction of natural soil deposits. For Camaldoli ash, the points representing the initial conditions of the natural deposit, characterized by void ratios around 1.1 and mean stress values of tens of kPa, are located well below the SSL (Figure 6). This suggests that the undrained behavior of the Camaldoli natural deposit is stable [23]. Thus, the experimental results show that, under undrained deformation, the Camaldoli ash, which has a particle size distribution

typical of potentially liquefiable natural deposits, is not subjected to an increase in pore pressure to be able to diminish the soil shear resistance, and therefore, it is not liquefiable.

4.1.2. Saturated Hydraulic Conductivity

The saturated conductivity of the soil, k_{sat}, was investigated through constant head permeability tests on natural samples. The results are shown in Figure 7. The values of k_{sat} are reported as a function of void ratio (Figure 7a) and the mean applied effective stress (Figure 7b). For a low state of stress, close to the in situ stress, the saturated permeability is about 10^{-5} m/s, which progressively decreases by an order of magnitude for applied effective stress as high as 700 KPa (Figure 7b).

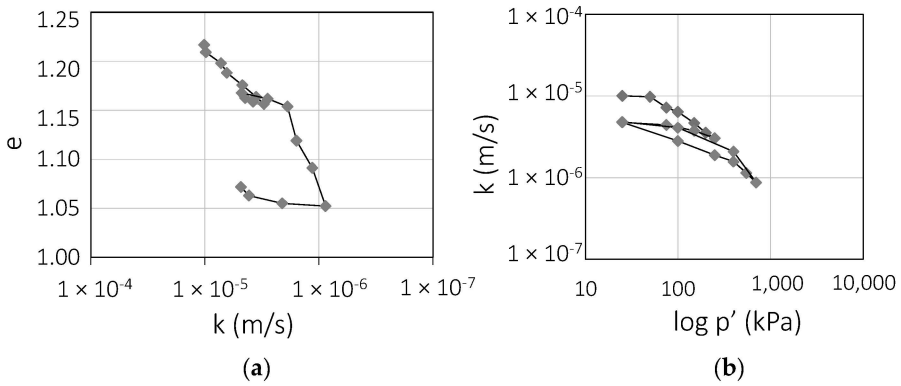

Figure 7. Saturated conductivity as a function of (**a**) void ratio and (**b**) mean effective stress.

4.2. Mechanical Properties in Unsaturated Conditions

Unsaturated soil properties play a key role in affecting the rate of rainwater infiltration and variation in the slope safety factor during a rainfall event. Therefore, to set up a physically based EWS, the proper characterization of the hydraulic and mechanical properties of unsaturated soil is crucial. The functional relationships used to interpret the experimental results, the corresponding parameters, and the procedures used in the following sections are extensively discussed in [1].

4.2.1. Shear Strength under Unsaturated Conditions (Sr < 1)

The experimental program was carried out in a suction-controlled triaxial cell (SCTX) on undisturbed specimens 70 mm in diameter by applying a mean net stress (T) of 50 and 100 kPa, and suction values ranging between 5 and 50 kPa (Table 3). The triaxial cell was equipped for internal measurements of axial deformation, carried out using LVDT transducers, radial mean deformation, and water volume exchanges through level transducers and a double burette system. Inside these instruments, both air flow and pore water flow were initiated through the upper and lower surfaces of the specimen to keep the imposed suction level constant, which was applied using the axis translation technique. After an equalization phase, needed to obtain a uniform suction distribution inside the specimen, an isotropic consolidation stage at constant suction was performed. Finally, the failure stage was induced by keeping the mean net stress and suction constant and progressively increasing the axial stress with a rate of 1.5 kPa/h to ensure a drained loading condition.

The test results are shown in the stress plane ($p–u_a$, q) in Figure 8a. In the same Figure, the critical state line corresponding to the saturated condition of the material (dashed line) is also reported. Thus, from the comparison, the mechanical effect of suction on the soil strength can be revealed. All the points representing failure in unsaturated conditions are located well above the failure envelope of the saturated soil, showing that suction in these soils plays a significant role.

Table 3. Triaxial tests in unsaturated conditions: initial conditions and applied state of stress.

SCTX	γ (kN/m^3)	γ_d (kN/m^3)	n (%)	e	$S_{r,f}$	$p-u_a$ (kPa)	u_a-u_w (kPa)
C_USP_1	15.2	11.8	52.50	1.104	0.64	50	5
C_USP_2	14.4	11.8	52.45	1.104	0.48	50	15
C_USP_3	13.6	11.8	52.47	1.105	0.34	50	35
C_USP_4	13.5	11.6	53.61	1.154	0.36	50	50
C_USP_5	14.2	11.8	52.46	1.105	0.44	100	5
C_USP_6	12.8	11.1	55.48	1.247	0.30	100	15
C_USP_7	15.4	11.4	54.96	1.192	0.74	100	35
C_USP_8	13.4	11.7	52.87	1.123	0.33	100	50

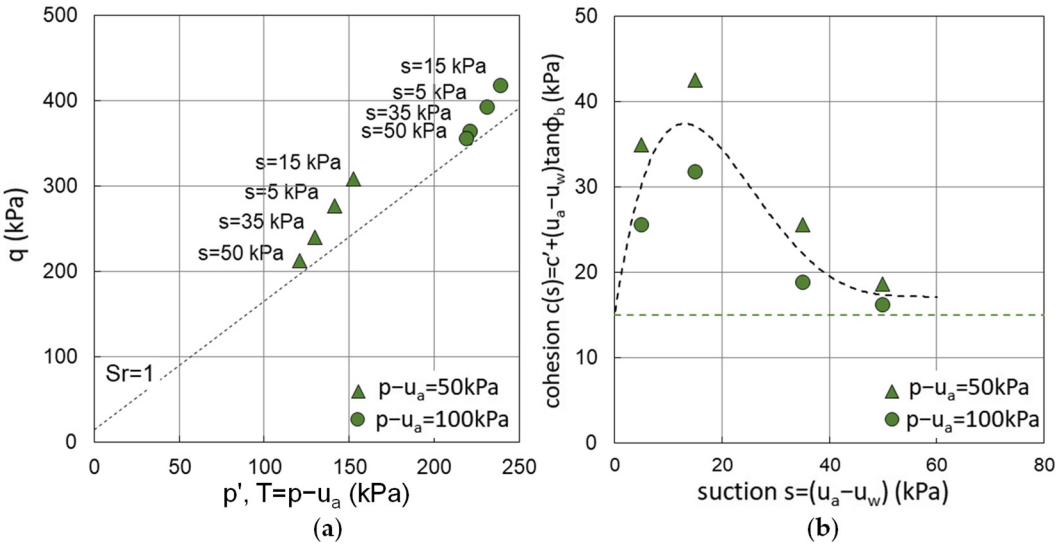

Figure 8. Unsaturated shear strength: (**a**) stress plane; (**b**) intercept of cohesion as a function of suction.

The results of the SCTX tests were also interpreted by using the extension of the Mohr–Coulomb criterion to the unsaturated soils proposed by [1], assuming a constant effective friction angle of 37°. The results, in terms of apparent cohesion as a function of matric suction, are illustrated in Figure 8b. The apparent cohesion, and hence the shear strength of the soil, increases at low matric suction until it reaches a peak for suction of about 15–18 kPa, and then it rapidly decreases. For values of suction higher than 50 kPa, the effect of suction on shear strength approaches a residual value ranging between 15 and 18 kPa, which should correspond to its effective value. Although the trends of the relationship between suction and apparent cohesion are similar for the two groups of specimens consolidated at different levels of mean net stresses, they are characterized by different magnitudes: the lower the mean net stress, the higher the effect of suction on shear strength. This can be ascribed to the different particle arrangements induced by the higher mean net stress that modifies the SWRC, especially at low suction values [24].

Nevertheless, the lowest values of the intercept of cohesion are sufficient to justify the stability of the slope with an inclination also higher than 40°.

4.2.2. Soil Water Retention Curve and Conductivity Function

To retrieve the SWRC of the Camaldoli ash in a range of suction from 0 up to 80 kPa, of primary interest for our research, an experimental set-up based on the evaporation method proposed by [25] was used. A sketch of the experimental apparatus is illustrated in Figure 9. The test was performed on a cubic sample of soil (10 × 10 × 10 cm^3), reconstituted with

an initial porosity of 0.55, by using two mini-tensiometers (jet-fill, Soil Moisture type) with ceramic tips located at different heights, and a TDR probe inserted horizontally at the mid-height of the specimen. Mini-tensiometers measure suction up to 100 kPa with an accuracy of 1 kPa. The TDR probe was used to measure the volumetric water content of the soil. It is based on the correlation between electric conductivity and water content. Taking advantage of the dielectric properties of the soil, the travel time of the electromagnetic pulse along the metal probes buried into the soil is measured and correlated to the volumetric water content [26]. An estimation of the volumetric water content was also carried out using gravimetric measurements by assuming a constant porosity in the soil sample (no significant volumetric changes and shrinkage occurred during the test).

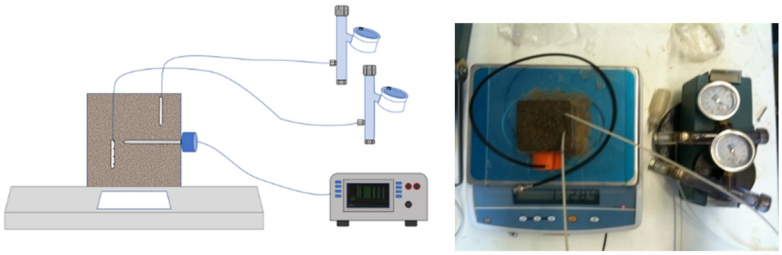

Figure 9. Sketch of the apparatus used for determination of the SWRC.

The test consisted of monitoring a series of evaporation and infiltration stages starting from an initial saturated condition. As there was no significant difference found by coupling the water content with matric suction measured at the most superficial or the deepest tensiometer, the two suction measurements were averaged to obtain the representative suction incurred by the specimen. The wetting and drying paths of the soil during the various phases are reported in Figure 10 by coupling suction measurements with the volumetric water content obtained using mass measurements. The experimental points obtained by coupling suction measurements with volumetric water content values retrieved with the TDR probe are also reported.

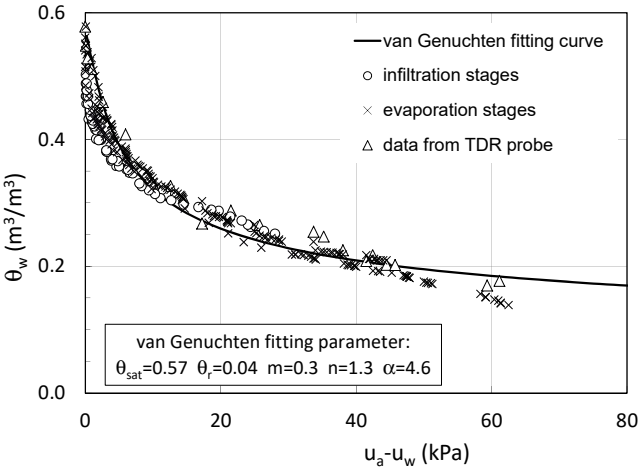

Figure 10. Soil water retention curve of the Camaldoli ash.

The Camaldoli ash has a negligible hydraulic hysteresis in the investigated range of suction, as the wetting and drying paths partly overlap. The obtained SWRC is typical of coarse soil, characterized by a very small air-entry value (in the order of a few kPa), a steep front in the transition zone, and a flatter trend approaching the residual zone of unsaturation. The experimental points were fitted by using the van Genuchten model [27]. The fitting parameters (α, n, m) are reported in Figure 10.

The hydraulic conductivity function (HCF) was analyzed using the SCTX tests. Each value was determined by analyzing the transient flow induced during the equalization

phase of an imposed suction level by using the Kunze expression [28]. Experimental values (green dots) are shown in Figure 11, along with the saturated conductivity values (white triangles). The same figure also shows another estimation of the unsaturated conductivities performed with the expression proposed by [29] based on the suction and saturation degrees measured at the end of each equalization phase. Finally, the trend of the permeability function determined with Gardner's function [30], which better approximates the experimental data, is depicted as a dashed line in Figure 11. In the investigated field of suction, hydraulic conductivity greatly reduces by about three orders of magnitude, reaching a value of about 1×10^{-8} m/s. For suction lower than 30 kPa, the data show a greater dispersion.

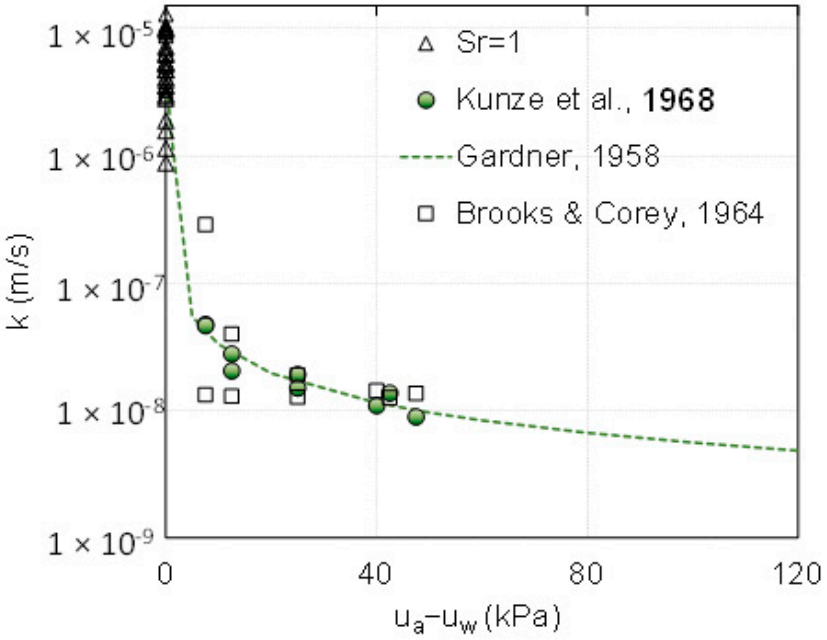

Figure 11. Hydraulic conductivity function of the Camaldoli ash (relationships for data interpretation from [28–30].

5. Discussion

The experimental results related to the Camaldoli soil can be incorporated into the soil database (SDB) on pyroclastic materials initially proposed by [9] for airfall deposition covers by adding information regarding volcanic ash belonging to a pyroclastic deposit of flow origin. The enriched SDB is reported in Figure 12, where data from the three study areas of Camaldoli, Cervinara, and Sarno are reported. In addition, to facilitate comparison and comments on the properties of these deposits, in Figure 13, the SWRCs (Figure 13a), HCFs (Figure 13b), apparent cohesion trends (Figure 13c), and undrained paths in the compression plane (Figure 13d) are shown.

The SDB is organized in the form of sheets where both geographical and geotechnical characteristics of a soil deposit are reported, together with an evaluation of the reliability of the most utilized literature expressions that were used to fit the experimental data.

The first section of the sheet indicates the site's geographical coordinates and some geomorphological data such as the average slope angle, the mean thickness of the cover, and the position within the stratigraphic sequence of the investigated layer from which undisturbed soil samples were taken and analyzed.

In the second section, the physical and state properties of the soil are reported. For the Camaldoli flow pyroclastic ash, the grain size distribution is located within the range of potentially liquefiable soil, and this information is highlighted in red in the SDB (Figure 12a) as a first indication of susceptibility to the liquefaction of the soil deposit.

In the third section of the sheet, the mechanical characteristics of the soil in saturated conditions are shown. In detail, the critical state parameters and the undrained behavior of the soil, evaluated through CIU triaxial tests on natural specimens consolidated in the range of stress acting in situ, are indicated. Once again, this latter information is highlighted in red in the case of an unstable soil response (liquefiable soil), yellow in the case of a partially unstable soil response, or green in the case of a stable undrained response.

Camaldoli pyroclastic soil

Geographical information and layer data

Latitude	Longitude	Average slope angle	Thickness cover	Thickness soil layer	Depth of the soil layer min	Depth of the soil layer max
N	E	[°]	[m]	[m]	[m]	[m]
40° 51' 30"	14° 11' 32"	50°	>10	0.5–2.00	1	1.5

Physical and state properties

Gs	n	γ_d	γ_{sat}
	%	[kN/m^3]	[kN/m^3]
2.49	54	10.7	16.6

Grain size distribution of liquefiable soil [yes or no]	yes

Saturated shear strength and critical state parameters

c'	ϕ'	M	λ
[kPa]	[°]		
10–15	37	1.53	0.1

Undrained unstable response in CTX tests [yes or no]	no

Unsaturated shear strength

mod. after Fredlund and Rahardjo 1993

c'	ϕ'	c(u_a-u_w)
[kPa]	[°]	[kPa]
10–15	37	*See Fig.8*

Evaluation of reliability	high

Lu et al. 2010

$\sigma_s = -(u_a - u_w)/[1+(\alpha(u_a - u_w))^n]^m$

α; n; m van Genuchten parameters

Evaluation of reliability	low

Permeability functions

Kunze et al. 1968

$k = 1/\alpha^2 \cdot L^2/V \cdot [Q_o/\Delta u_o] \cdot \rho_w \cdot g \cdot b_\alpha$

b_α from analysis of suction equalization (SCTX)

ks [S_r=1]	k_P	L_P	$\alpha = L_P/K_P \cdot k/L$
[m/s]	[m/s]	[mm]	
4.50 × 10^{-6}	1 × 10^{-7}	5	

Evaluation of reliability	high

Brooks and Corey 1964

$k = ks$ if $(u_a - u_w) \leq (u_a - u_w)_b$

$k = ks * S_e^{\eta}$ if $(u_a - u_w) \leq (u_a - u_w)_b$

$\eta = 2 + 3\lambda$; λ=pore size distribution index

ks [S_r=1]	$(ua-uw)_b$	λ	η
[m/s]	[kPa]	[-]	[-]
4.50 × 10^{-6}	1	0.45	3.35

Evaluation of reliability	low

Gardner 1958

$k = ks/[1 + a\,[(u_a - u_w)/\rho g]^n]$

ks [S_r=1]	a	n
[m/s]	[-]	[-]
4.50 × 10^{-6}	1	0.87

Evaluation of reliability	medium

Water retention curves

van Genuchten 1980

$(\theta - \theta_r)/(\theta_s - \theta_r) = [1/(1+(\alpha h)^n)]^m$

h=pressure head assumed positive [m]

θ_s	θ_r	α	n	m
		[1/m]		
0.57	0.04	4.6	1.3	0.3

Evaluation of reliability	high

(**a**)

Figure 12. *Cont.*

Cervinara pyroclastic soil

Geographical information and layer data

Latitude	Longitude	Average slope angle	Thickness cover	Thickness soil layer	Depth of the soil layer min	Depth of the soil layer max
N	E	[°]	[m]	[m]	[m]	[m]
41° 00' 28"	14° 38' 38"	38°	2.2	0.6–1.4	0.8	1.8

Physical and state properties

Gs	n	γ_d	γ_{sat}
	%	[kN/m^3]	[kN/m^3]
2.58	69	8.0	14.8

Grain size distribution of liquefiable soil [yes or no]	yes

Saturated shear strength and critical state parameters

c'	ϕ'	M	λ
[kPa]	[°]		
0	38	1.55	0.19

Undrained unstable response in CTX tests [yes or no]	yes

Unsaturated shear strength

mod. after Fredlund and Rahardjo 1993

c'	ϕ'	$c(u_a-u_w)$
[kPa]	[°]	[kPa]
0	38	if $(u_a-u_w)\leq 1$ 0 if $(u_a-u_w)>1$ $2.4\ln(u_a-u_w)$

Evaluation of reliability	high

Lu et al. 2010

$\sigma_s=-(u_a-u_w)/[1+(\alpha(u_a-u_w))^n]^m$

α; n; m van Genuchten parameters

Evaluation of reliability	medium

Permeability functions

Kunze et al. 1968

$k= 1/\alpha^2 \cdot L^2/V \cdot [Q_o/\Delta u_o] \cdot \rho_w \cdot g \cdot b_\alpha$

b_α from analysis of suction equalization (SCTX)

ks [S_r=1] [m/s]	k_P [m/s]	L_P [mm]	$\alpha=L_P/K_P \cdot k/L$
3.70×10^{-7}	1×10^{-7}	5	

Evaluation of reliability	high

Brooks and Corey 1964

$k=ks$ if $(u_a-u_w)\leq(u_a-u_w)_b$

$k=ks[(u_a-u_w)_b/(u_a-u_w)]^\eta$ if $(u_a-u_w)\leq(u_a-u_w)_b$

$\eta=2+3\lambda$; λ=pore size distribution index

ks [S_r=1] [m/s]	$(ua-uw)_b$ [kPa]	λ [–]	η [–]
3.70×10^{-7}	1	0.39	3.17

Evaluation of reliability	low

Gardner 1958

$k=ks/[1+a\,[(u_a-u_w)/\rho g]^n]$

ks [S_r=1] [m/s]	a [–]	n [–]
3.70×10^{-7}	1	0.8

Evaluation of reliability	medium

Water retention curves

van Genuchten 1980

$(\theta-\theta_r)/(\theta_s-\theta_r)=[1/(1+(\alpha h)^n)]^m$

h=pressure head assumed positive [m]

θ_s	θ_r	α [1/m]	n	m
0.7	0.17	1	0.47	1.5

Evaluation of reliability	high

(**b**)

Figure 12. *Cont.*

Sarno pyroclastic soil

Geographical information and layer data

Latitude	Longitude	Average slope angle	Thickness cover	Thickness soil layer	Depth of the soil layer min	Depth of the soil layer max
N	E	[°]	[m]	[m]	[m]	[m]
40° 50' 45"	14° 36' 42"	40°	3.5	0.8–2.0	1	2.6

Physical and state properties

Gs	n	γ_d	γ_{sat}
	%	[kN/m^3]	[kN/m^3]
2.61	68	8.3	15.5

Grain size distribution of liquefiable soil [yes or no]	yes

Saturated shear strength and critical state parameters

c'	ϕ'	M	λ
[kPa]	[°]		
0	37	1.51	0.12

Undrained unstable response in CTX tests [yes or no]	yes

Unsaturated shear strength

mod. after Fredlund and Rahardjo 1993

c'	ϕ'	c(u_a-u_w)	
[kPa]	[°]	[kPa]	
		if $(u_a-u_w)\leq 1$	0
0	37	if $(u_a-u_w)>1$	$1.8\ln(u_a-u_w)$

Evaluation of reliability	high

Lu et al. 2010

$\sigma_s=-(u_a-u_w)/[1+(\alpha(u_a-u_w))^n]^m$

α; n; m van Genuchten parameters

Evaluation of reliability	medium

Permeability functions

Kunze et al. 1968

$k= 1/\alpha^2 \cdot L^2/V \cdot [Q_o/\Delta u_o] \cdot \rho_w \cdot g \cdot b_\alpha$

b_α from analysis of suction equalization (SCTX)

ks [S_r=1]	k_P	L_P	$\alpha=L_P/K_P \cdot k/L$
[m/s]	[m/s]	[mm]	
6×10^{-7}	1×10^{-7}	5	

Evaluation of reliability	high

Brooks and Corey 1964

$k=ks$ if $(u_a-u_w)\leq(u_a-u_w)_b$

$k=ks[(u_a-u_w)_b/(u_a-u_w)]^\eta$ if $(u_a-u_w)\leq(u_a-u_w)_b$

$\eta=2+3\lambda$; λ=pore size distribution index

ks [S_r=1]	$(ua-uw)_b$	λ	η
[m/s]	[kPa]	[-]	[-]
6×10^{-7}	1.1	0.45	3.35

Evaluation of reliability	low

Gardner 1958

$k=ks/[1+a\,[(u_a-u_w)/\rho g]^n]$

ks [S_r=1]	a	n
[m/s]	[−]	[−]
6×10^{-7}	1	0.87

Evaluation of reliability	medium

Water retention curves

van Genuchten 1980

$(\theta-\theta_r)/(\theta_s-\theta_r)=[1/(1+(\alpha h)^n)]^m$

h=pressure head assumed positive [m]

θ_s	θ_r	α	n	m
		[1/m]		
0.7	0.18	0.9	0.45	1.4

Evaluation of reliability	high

(**c**)

Figure 12. Database of soil characteristics: (**a**) Camaldoli flow deposit; (**b**) Cervinara airfall deposit; (**c**) Sarno airfall deposit (literature expressions from [1,27–31]).

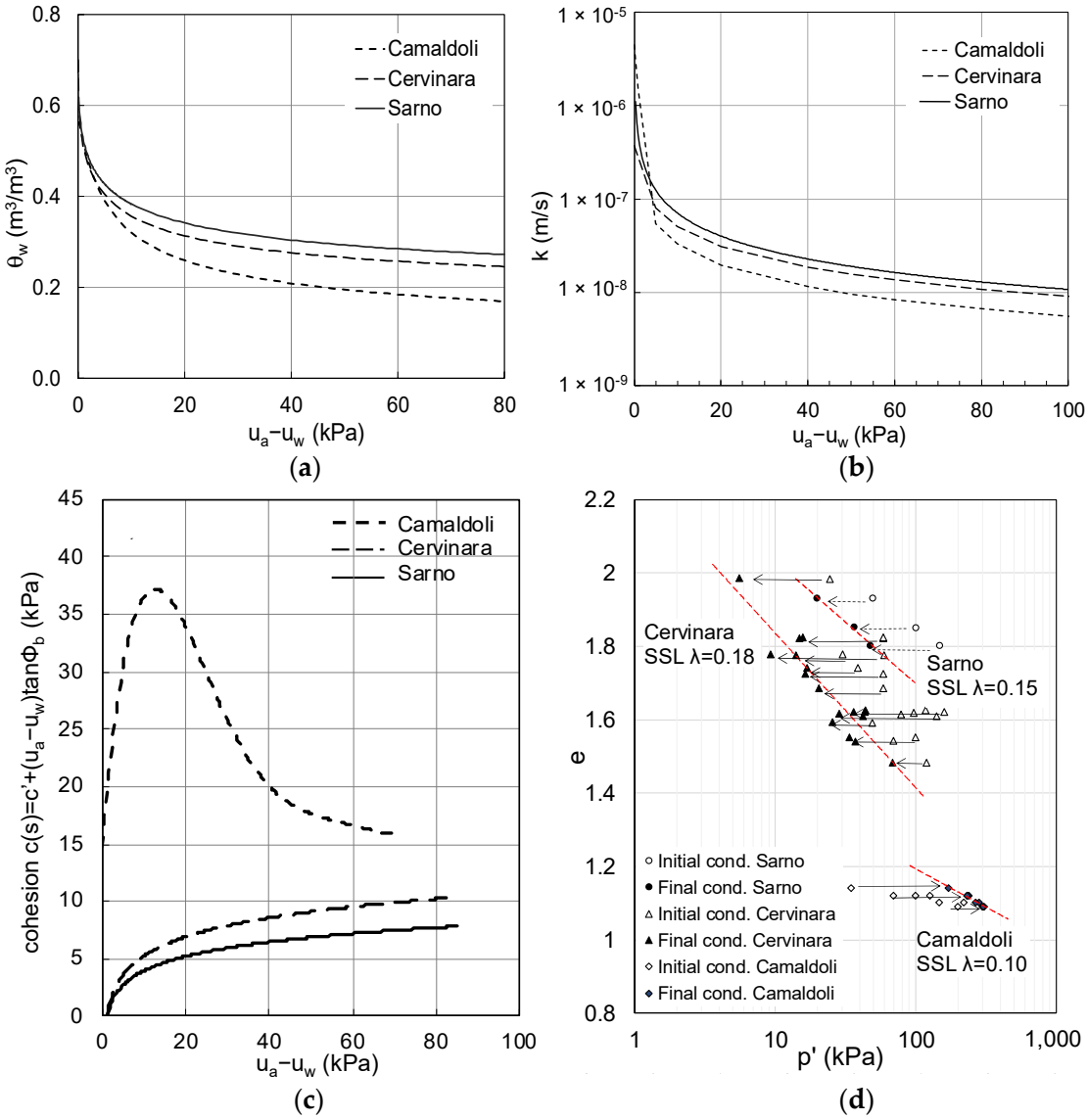

Figure 13. Comparison of the mechanical properties of three investigated pyroclastic deposits: (**a**) SWRCs; (**b**) HCFs; (**c**) apparent cohesion trends; and (**d**) undrained paths in the compression plane.

Afterward, a section that synthetizes the unsaturated shear strength in terms of the functional relationship between suction and apparent cohesion is provided. When a simple unique trend for this relationship is not found, as is the case for the Camaldoli ash, the information in the box reports the experimental points illustrated in the figure. In this section, the reliability of the expression proposed by [32], which is widely used in the literature for the evaluation of the unsaturated shear strength of granular soils, is also determined.

Finally, the last section of the SDB reports the hydraulic properties of the soil. The parameters of various expressions reported in the literature for soil water retention curves and the hydraulic conductivity function that best fits the experimental data are indicated therein.

Based on the data collected in the SDB and illustrated in Figure 13, the properties of the Camaldoli flow deposit are different from those of the Cervinara and Sarno airfall deposits. Although the three deposits are characterized by similar trends of hydraulic properties (Figure 13a,b), greater differences arise when we look at the shear strength in both unsaturated and saturated states. Indeed, under unsaturated conditions, the soil from the flow deposit shows a trend of apparent cohesion intercept very different from that of the airfall ash deposits, and they are also characterized by higher values (Figure 13c).

Despite the similar grain size distribution of the three deposits, which has a great influence on the relationship between suction and unsaturated shear strength [31,32], the significant difference observed in the experimentally obtained functions must be attributed to the dissimilar formation of the two kinds of deposits.

Analyzing the mechanical properties of the soils under saturated conditions, it can be seen that the effective friction angles of the three deposits are very similar ranging between 37 and 38°, but the flow ash deposit presents an effective cohesion of few kPa, as reported in the SBD (Figure 12). Considering the soil response under undrained loading, framed within the steady-state theory and illustrated in the compression plane of Figure 13d, various behaviors can be recognized. Firstly, the locations of the SSLs are very different, which is related to the dissimilar void ratios of the natural deposits (around 1.9 for fall deposits and 1.1 for flow deposits). The SSLs of the airfall ash deposits localize in the upper part of the compression plane, presenting a high inclination ($\lambda = 0.19$ for Cervinara and $\lambda = 0.12$ for Sarno), whereas the SSL of the flow ash deposit is located in the lower part and characterized by a lower inclination. More importantly, the undrained responses of the three deposits are significantly different. In the range of stresses that the soils may potentially experience at failure in situ after soil saturation, the undrained paths of the airfall deposits show an unstable behavior, differently from the flow deposit, which shows a stable behavior (de Cristofaro et al., 2022). Flow or surge deposits, characterized by lower porosity than airfall ash deposits, do not show a tendency toward liquefaction under the actual in situ stress level. In fact, by evaluating the state parameter ψ defined by [33] using the state conditions at the end of the consolidation stage of the CIU test in the range of p' representing in situ conditions ($20 < p' < 50$ kPa; $e = 1.14$ for Camaldoli; $e = 1.98$ for Cervinara; $e = 1.93$ for Sarno), it can be seen that it assumes a negative value for the Camaldoli ash soil (about -0.20), which represents a non-liquefiable deposit, whereas it assumes positive values ($0.13 \div 0.31$) for both the Cervinara and Sarno soils, indicative of a liquefiable deposit.

Again, these characteristics can be attributed to the different deposition modes of the materials: in the case of a flow deposit, a medium porosity soil structure results in a stable behavior in an undrained loading process. In contrast, the eolian transport over long distances, followed by slow fall deposition in the carbonatic context, allows for the formation of an open-spaced metastable soil structure characterized by porosity values as high as 70%, which leads to an unstable undrained response and a loss of shear resistance.

Assessment of the Post-Failure Evolution of Landslides in Pyroclastic Covers

Data collected in the SDB constitute the basic and essential information required not only to implement a physically based model for the analysis of the infiltration process and analyze the slope stability in a boundary value problem but also for forecasting the post-failure evolution of landslides. Indeed, data presented in the SDB of Figure 12, along with the flowchart illustrated in Figure 14, can be used in an EWS as a supporting tool for the identification of the post-failure evolution of rainfall-induced landslides in pyroclastic shallow covers of Campania. The flowchart is organized into two sections. The first concerns checking the degree of saturation of soil at the onset of instability as it is the discriminator between the potential development of a drained or undrained soil response, whereas the second allows for the assessment of the post-failure evolution of the sliding mass based on the information reported in the SDB.

The flowchart, originally proposed by [3] for cohesionless soils, was modified to extend the analysis to granular covers characterized by small values of cohesion, as in the case of the Camaldoli hill. In the simplified assumption of infinite slope and cohesionless soil, the degree of saturation at failure can be easily determined by comparing the acclivity of the slope with the effective friction angle: for slope inclination less or equal to the friction angle of the soil (gentle or steep slope) failure occurs in saturated conditions, whereas for slope inclination higher than the friction angle (very steep slope), failure involves partially saturated soil. However, in the case of soils with effective cohesion, it is not possible to

assess the degree of saturation at failure simply by comparing the friction angle with the slope angle. Moreover, differently from the case of cohesionless soil, the safety factor is no longer independent from the depth, decreasing with an increase in depth and introducing another variable, the depth of the sliding surface, to the equilibrium analysis. Therefore, the critical slope angle (α_{crit}) is introduced instead of the slope angle (α), defined as the slope inclination at which failure occurs under saturated conditions. This critical angle must be determined case by case, eventually assuming a simplified hypothesis. Obviously, for homogeneous cohesionless soils, the critical slope angle is equal to the friction angle of the material.

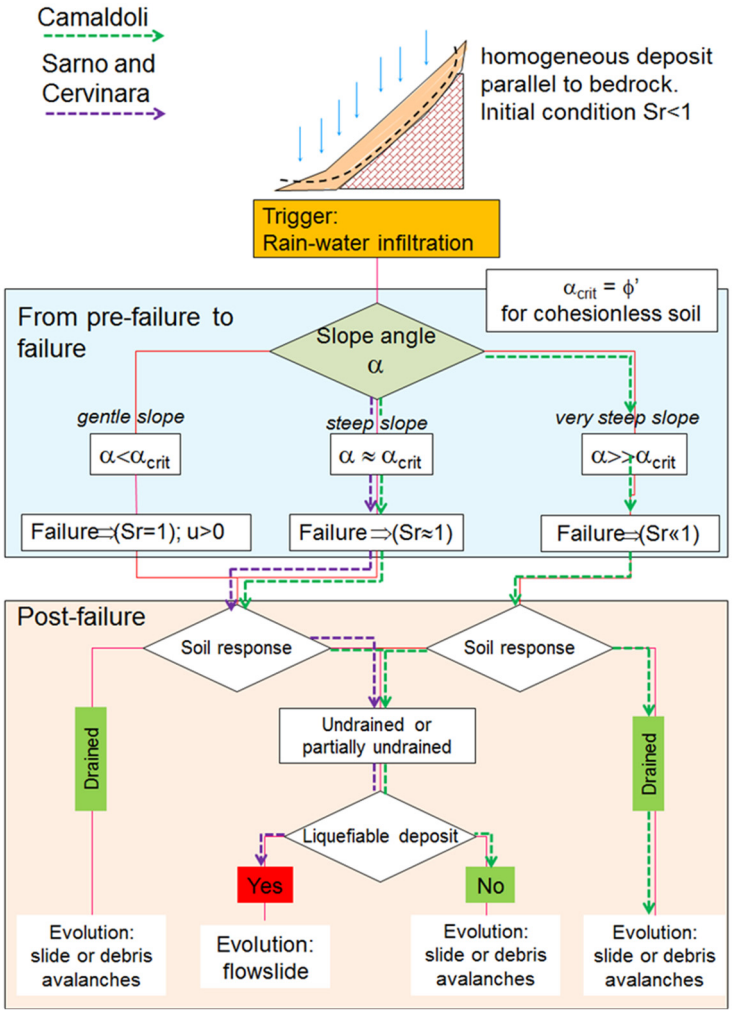

Figure 14. Flowchart for simplified assessment of the post-failure evolution of landslides in granular soils (red box highlights the potential post-failure evolution in flowslide; green boxes denote evolution in slide or debris avalanches).

Here, an example of the application of this method for the three investigated sites is proposed. The analysis starts with the evaluation of the degree of saturation of soil at failure. In the case of Cervinara and Sarno cohesionless soil deposits, which have effective friction angles close to the inclination of the slopes ($\phi' \approx \alpha_{crit}$), failure occurs in an almost saturated condition. In the flowchart, the path to be followed (purple line) is the one corresponding to a steep slope ($\alpha \approx \alpha_{crit}$).

In the case of Camaldoli hill, as the soil presents an intercept of effective cohesion, the first step consists of the evaluation of α_{crit}. Based on the observation of detachment areas, which shows that the sliding surfaces are located at about 1.5 m of depth, α_{crit} is determined by performing stability analysis at different inclinations of the slope, in the

simplified hypothesis of a constant suction profile and by using the peak state parameters ($\phi' = 38^\circ$ and $c' = 15$ kPa). The analysis results show that it corresponds to a slope inclination of 65°: In the presence of α lower than α_{crit}, slope failure occurs in saturated conditions; for α higher than α_{crit}, the mobilization of the soil deposit occurs in soil which is still in unsaturated conditions. Along the Camaldoli hill, slope instabilities mainly involve the upper part of the slope above the vertical tuff cliff where soil deposits present local acclivity higher than 60°. Thus, instability may occur regardless of whether the soil is saturated or not: the potential paths to follow in the flowchart (green lines) correspond to both the last two branches related to the steep slope ($\alpha \approx \alpha_{crit}$) and very steep slope ($\alpha \approx \alpha c_{rit}$).

Afterward, the assessment of the post-failure evolution of the landslide can be carried out by looking at the second part of the flowchart. If the post-failure movement occurs in a drained condition, landslide phenomena evolve into slide or debris avalanche; if it occurs under undrained or partially undrained conditions, the evolution of the landslide is related to soil susceptibility to liquefaction.

In the case of the Sarno and Cervinara deposits, as evaluated through infiltration tests in small-scale slopes reconstituted in a multi-instrumented flume [34,35], in the very early post-failure stage, soils exhibit an undrained response, as evidenced by the high excess pore pressures observed. Thus, we can infer that the path to follow in the flowchart is the one corresponding to an undrained or partially undrained response, which, in the presence of such liquefiable deposits, leads to the prediction of evolution into a flowslide.

Different is the case of the Camaldoli slope. Indeed, although we cannot predict if a drained or undrained condition will occur at the onset of failure because the deposit is non-liquefiable, the slope movement will evolve into a slide or a debris avalanche.

In fact, as reported by [14], a significant feature of most landslides occurring in pyroclastic deposits in the volcanic context is the absence of any signs of liquefaction.

6. Conclusions

A wide mountainous area in Campania (southern Italy) is threatened by rainfall-induced landslides, which mainly affect the granular pyroclastic covers and evolve into rapid slides, debris avalanches, or catastrophic flowslides deeply affecting urban developments at the foot slope. For these densely urbanized areas, knowledge of both the landslide susceptibility of the territory and the type of evolution of the landslide mass, which can impact the exposed areas in a very different way, is mandatory.

To this end, in this paper, an extensive testing program was developed to investigate both unsaturated and saturated mechanical properties and evaluate soil susceptibility to liquefaction of volcanic ash belonging to a flow deposit, frequently involved in debris avalanches. Moreover, the properties of other types of ash belonging to airfall deposits, involved in flowslides, were compared to highlight the similarities and dissimilarities between the two types of deposits and explain the different patterns of the post-failure evolution of the landslide mass. Based on the experimental results, a soil database for hydro-geotechnical models was presented, which contains all the data needed for an advanced constitutive soil modeling to implement a physically based model for forecasting the initiation of landslides, thus improving the effectiveness of early warning systems. In addition, a framework was proposed for the assessment of landslide evolution under a simplified hypothesis that can be used by stakeholders for land management and the protection of areas at risk.

Author Contributions: Conceptualization, E.D. and L.O.; methodology, E.D. and L.O.; formal analysis, all authors; investigation, M.d.C., L.I., G.C. and A.B.; data curation, M.d.C. and L.I.; writing—original draft preparation, E.D. and L.I.; writing—review and editing, all authors; supervision, E.D. and L.O.; funding acquisition, L.O. All authors have read and agreed to the published version of the manuscript.

Funding: This research was funded by the Program VALERE: "VAnviteLli pEr la RicErca", DDG n. 516–24/05/2018.

Data Availability Statement: The data used in this research work are available upon request from the corresponding authors.

Conflicts of Interest: The authors declare no conflict of interest.

References

1. Fredlund, D.G.; Rahardjo, H. Shear Strength Theory. In *Soil Mechanics for Unsaturated Soils*; Wiley: New York, NY, USA, 1993; pp. 217–259. [CrossRef]
2. Cascini, L.; Cuomo, S.; Guida, D. Typical source areas of May 1998 flow-like mass movements in the Campania region, Southern Italy. *Eng. Geol.* **2008**, *96*, 107–125. [CrossRef]
3. Damiano, E.; Olivares, L. The role of infiltration processes in steep slope stability of pyroclastic granular soils: Laboratory and numerical investigation. *Nat. Hazards* **2010**, *52*, 329–350. [CrossRef]
4. Sorbino, G.; Nicotera, M.V. Unsaturated soil mechanics in rainfall-induced flow landslides. *Eng. Geol.* **2013**, *165*, 105–132. [CrossRef]
5. De Vita, P.; Di Clemente, E.; Rolandi, M.C.P. Engineering geological models of the initial landslides occurred on April 30, 2006, at Monte Vezzi (Ischia Island, Italy). *Ital. J. Eng. Geol. Environ.* **2007**, *2*, 119–141.
6. Olivares, L.; Damiano, E.; Mercogliano, P.; Picarelli, L.; Netti, N.; Schiano, P.; Savastano, V.; Cotroneo, F.; Manzi, M.P. A simulation chain for early prediction of rainfall-induced landslides. *Landslides* **2014**, *11*, 765–777. [CrossRef]
7. Cascini, L.; Cuomo, S.; Pastor, M.; Sorbino, G. Modeling of Rainfall-Induced Shallow Landslides of the Flow-Type. *J. Geotech. Geoenviron. Eng.* **2010**, *136*, 85–98. [CrossRef]
8. Marino, P.; Santonastaso, G.F.; Fan, X.; Greco, R. Prediction of shallow landslides in pyroclastic-covered slopes by coupled modeling of unsaturated and saturated groundwater flow. *Landslides* **2021**, *18*, 31–41. [CrossRef]
9. Olivares, L.; Damiano, E.; Netti, N.; de Cristofaro, M. Geotechnical properties of two pyroclastic deposits involved in catastrophic flowslides for implementation in early warning systems. *Geosciences* **2019**, *9*, 24. [CrossRef]
10. Olivares, L.; Picarelli, L. Shallow flowslides triggered by intense rainfalls on natural slopes covered by loose unsaturated pyroclastic soils. *Geotechnique* **2003**, *53*, 283–287. [CrossRef]
11. Picarelli, L.; Olivares, L.; Lampitiello, S.; Darban, R.; Damiano, E. The undrained behaviour of an air-fall volcanic ash. *Geosciences* **2020**, *10*, 60. [CrossRef]
12. de Falco, M.; Di Crescenzo, G.; Santo, A. Volume estimate of flow-type landslides along carbonatic and volcanic slopes in Campania (Southern Italy). *Nat. Hazards* **2012**, *61*, 51–63. [CrossRef]
13. Picarelli, L.; Evangelista, A.; Rolandi, G.; Paone, A.; Nicotera, M.V.; Olivares, L.; Scotto di Santolo, A.; Lampitiello, S.; Rolandi, M. Mechanical Properties of Pyroclastic Soils in Campania Region. In Proceedings of the 2nd International Workshop on Characterization and Engineering Properties of Natural Soils, Singapore, 29 November–1 December 2006; Volume 4, pp. 2331–2384.
14. Picarelli, L.; Olivares, L.; Damiano, E.; Darban, R.; Santo, A. The effects of extreme precipitations on landslide hazard in the pyroclastic deposits of Campania Region: A review. *Landslides* **2020**, *17*, 2343–2358. [CrossRef]
15. Calcaterra, D.; Coppin, D.; de Vita, S.; Di Vito, M.; Orsi, G.; Palma, B.; Parise, M. Slope processes in weathered volcaniclastic deposits within the city of Naples: The Camaldoli Hill case. *Geomorphology* **2007**, *87*, 132–157. [CrossRef]
16. de Falco, M.; di Crescenzo, G.; Santo, A. Empirical relationships to predict the runout of flow-type landslides in pyroclastic deposits in Campania region (Southern Italy). *Rend. Online Soc. Geol. Ital.* **2013**, *24*, 86–88.
17. Zona, R.; de Cristofaro, M.; Esposito, L.; Ferla, P.; Palladino, S.; Totaro, E.; Olivares, L.; Minutolo, V. Early warning system for landslide risk and SHM by means of reinforced optic fiber in lifetime strain analysis. In Proceedings of the 5th International Conference on Internet of Things, Big Data and Security, Prague, Czech Republic, 7–9 May 2020. [CrossRef]
18. Minutolo, V.; Cerri, E.; Coscetta, A.; Damiano, E.; De Cristofaro, M.; Di Gennaro, L.; Esposito, L.; Ferla, P.; Mirabile, M.; Olivares, L.; et al. NSHT: New smart hybrid transducer for structural and geotechnical applications. *Appl. Sci.* **2020**, *10*, 4498. [CrossRef]
19. Hunter, G.; Fell, R. Prediction of impending failure of embankments on soft ground. *Can. Geotech. J.* **2003**, *40*, 209–220. [CrossRef]
20. Olivares, L.; Picarelli, L. Occurrence of flowslide in soils of pyroclastic origin and considerations for landslide hazard mapping. In Proceedings of the Fourteenth Southeast Asian Geotechnical Conference, Hong Kong, China, 14 December 2001.
21. Carrieri, G. Caratterizzazione di Depositi Piroclastici Saturi e Parzialmente Saturi. Ph.D. Thesis, Seconda Università degli Studi di Napoli, Caserta, Italy, 2013. [CrossRef]
22. Poulos, S.J.; Castro, G. Liquefaction Evaluation Procedure. *J. Geotech. Eng.* **1985**, *111*, 772–792. [CrossRef]
23. de Cristofaro, M. Essential Elements to Define Early Warning Systems in Volcanic Deposits. Ph.D. Thesis, University of Campania 'Luigi Vanvitelli', Caserta, Italy, 2022.
24. Lee, I.-M.; Sung, S.-G.; Cho, G.-C. Effect of stress state on the unsaturated shear strength of a weathered granite. *Can. Geotech. J.* **2005**, *42*, 624–631. [CrossRef]
25. Schindler, U.; Müller, L. Simplifying the evaporation method for quantifying soil hydraulic properties. *J. Plant Nutr. Soil Sci.* **2006**, *169*, 623–629. [CrossRef]
26. Topp, G.C.; Davis, J.L.; Annan, A.P. Electromagnetic determination of soil water content: Measurements in coaxial transmission lines. *Water Resour. Res.* **1980**, *16*, 574–588. [CrossRef]

27. van Genuchten, M.T. A Closed-form Equation for Predicting the Hydraulic Conductivity of Unsaturated Soils. *Soil Sci. Soc. Am. J.* **1980**, *44*, 892–898. [CrossRef]
28. Kunze, R.J.; Uehara, G.; Graham, K. Factors Important in the Calculation of Hydraulic Conductivity. *Soil Sci. Soc. Am. J.* **1968**, *32*, 760–765. [CrossRef]
29. Brooks, R.; Corey, A. *Hydraulic Properties of Porous Media*; Hydrology Papers; Colorado State University: Fort Collins, CO, USA, 1964.
30. Gardner, W.R. Some steady-state solutions of the unsaturated moisture flow equation with application to evaporation from a water table. *Soil Sci.* **1958**, *85*, 228–232. [CrossRef]
31. Lu, N.; Godt, J.W.; Wu, D.T. A closed-form equation for effective stress in unsaturated soil. *Water Resour. Res.* **2010**, *46*. [CrossRef]
32. Lu, N.; Likos, W.J. Suction Stress Characteristic Curve for Unsaturated Soil. *J. Geotech. Geoenviron. Eng.* **2006**, *132*, 131–142. [CrossRef]
33. Been, K.; Jefferies, M.G. A state parameter for sands. *Géotechnique* **1985**, *35*, 99–112. [CrossRef]
34. Darban, R.; Damiano, E.; Minardo, A.; Olivares, L.; Picarelli, L.; Zeni, L. An Experimental Investigation on the Progressive Failure of Unsaturated Granular Slopes. *Geosciences* **2019**, *9*, 63. [CrossRef]
35. Damiano, E.; Darban, R.; Olivares, L.; Picarelli, L. An investigation on progressive failure in granular slopes leading to flow-like landslides. In Proceedings of the 13th International Symposium on Landslides, Cartagena, Colombia, 15–19 June 2020.